CHEMICAL PHYSICS

State-to-state chemistry for three-body recombination in an ultracold rubidium gas

Joschka Wolf,[1] Markus Deiß,[1] Artjom Krükow,[1] Eberhard Tiemann,[2] Brandon P. Ruzic,[3] Yujun Wang,[4] José P. D'Incao,[5] Paul S. Julienne,[3] Johannes Hecker Denschlag[1]*

Experimental investigation of chemical reactions with full quantum state resolution for all reactants and products has been a long-term challenge. Here we prepare an ultracold few-body quantum state of reactants and demonstrate state-to-state chemistry for the recombination of three spin-polarized ultracold rubidium (Rb) atoms to form a weakly bound Rb_2 molecule. The measured product distribution covers about 90% of the final products, and we are able to discriminate between product states with a level splitting as small as 20 megahertz multiplied by Planck's constant. Furthermore, we formulate propensity rules for the distribution of products, and we develop a theoretical model that predicts many of our experimental observations. The scheme can readily be adapted to other species and opens a door to detailed investigations of inelastic or reactive processes.

Although the quantum mechanical principles underlying chemical reactivity are known, calculating the full state-to-state dynamics is only possible when the number of product exit channels is very limited (*1*–*3*). In a typical chemical reaction, however, where hundreds of molecular states are involved, a direct solution is currently beyond reach. Experimental investigations of state-to-state processes are challenging, as both the preparation of the reactants and the detection of the products have to take place in a quantum state–resolved manner. Until now, state-to-state experiments have typically been carried out with atomic and molecular beams [for reviews, see, e.g., (*4*–*6*)]. These studies are restricted to collisions between only two particles, owing to low densities. Furthermore, the collision energies are such that many partial waves are involved, and hyperfine states are generally not resolved.

Three-body recombination is an exothermic reaction, whereby three atoms collide to form a diatomic molecule and a free atom, each of which carries away a portion of the released kinetic energy (*7*–*9*). These reactions strongly depend on the collision energy, the initial quantum state of the reactants, and the details of their interactions. Ultracold atomic gases are amenable to extraordinary control of these parameters (*10*–*12*), enabling studies that determine the scaling properties of the total three-body recombination [see, e.g., (*13*–*21*)]. In principle, there is a wide range of molecular states that can be formed, ranging from weakly to deeply bound. To form a molecule with a given bond length, the three atoms need to approach each other within roughly one bond length. Because for dilute gases three-body collisions happen more frequently at long distances than at short ones, the formation of weakly bound molecules with long bonds is favored (*19*). At ultracold temperatures, the scattering length sets a typical length scale for the minimal distance between the reactants as they pass each other in a collision. Indeed, early investigations of three-body recombination showed that, for resonant interactions (large scattering lengths), molecules formed almost exclusively in the most weakly bound state, which has a typical size given by the scattering length (*22*, *23*). For nonresonant interactions (small scattering lengths), a population of more deeply bound molecular states is also expected, and it remains an open question how sensitive the product distribution is to the details of the interaction potential (*24*, *25*).

Here we demonstrate state-to-state chemistry for three-body recombination at ultralow temperatures. The experiments were carried out with a gas of ultracold ^{87}Rb atoms with nonresonant interactions confined in a crossed optical dipole trap (*26*). Each atom was in the electronic ground state, with total angular momentum and magnetic quantum numbers $f = 1$ and $m_f = -1$, respectively. Three-body recombination produced Rb_2 molecules in the mixed $X^1\Sigma_g^+$ and $a^3\Sigma_u^+$ electronic state manifolds. In a recent precursor experiment (*27*), we observed the first signals of such Rb_2 product states and could tentatively assign some of them. To reach the realm of state-to-state chemistry, we have now overcome the limitations of this first experiment by extending the detection scheme as well as the analysis. The assignment of the observed lines is now unambiguous, and we have developed a method to calibrate the flux into each final product state. Furthermore, instead of only probing isolated vibrational levels, we can now investigate the population distribution over a sequence of vibrational levels, covering about 90% of all produced molecules. On the basis of this technical progress, we gained a number of new scientific results and were able to formulate several propensity rules. Furthermore, we have carried out a state-of-the-art parameter-free model calculation that can be directly compared to our data and is a key tool for their interpretation.

To detect the molecular product quantum states, we ionized the newly formed molecules in a state-selective fashion using a two-color (1, 2) resonance-enhanced multiphoton ionization (REMPI) technique. Subsequently, the ions were captured in a Paul trap. After a given delay, during which several ions accumulated, we counted them. Figure 1A shows the two-color REMPI scheme. By tuning the frequency of the probe laser (*26*), we state-selectively excited weakly bound molecules to the $v' = 66$ vibrational level of the $A^1\Sigma_u^+$ potential [for selection rules, see (*26*)]. This level exhibits a simple rotational substructure (*28*, *29*) (see inset, Fig. 1A) with predicted hyperfine splittings of less than 3 MHz. From there, two photons from an ionization laser ionized the molecule (*26*). In Fig. 1B, we plot the term energies of the most relevant weakly bound molecular levels with $F = 2$ for the atom pair $f_a = 1, f_b = 1$, where the indices represent atoms a and b and F denotes the total angular momentum of the molecule excluding its rotational angular momentum R. The term energies were obtained from coupled-channel calculations (*26*).

As preparation for the assignment of the product states, we first calibrated the probe laser frequency with respect to the term energies of the probed weakly bound levels by carrying out a photoassociation measurement (*30*) that sets a marker for zero binding energy. The ion trap was turned off, and the probe laser frequency ν was scanned in small steps of 5 MHz while the dipole trap laser was kept at a fixed frequency. For every step, we exposed a freshly prepared atom cloud to the probe laser for a duration of 2 s and afterward measured the remaining number of atoms N using absorption imaging. On resonance, the probe laser couples two ultracold Rb atoms colliding in a s-wave (i.e., $R = 0$) to the bound level $A^1\Sigma_u^+$, $v' = 66$, $J' = 1$, and atom loss occurs. Here, J' is the total angular momentum quantum number excluding nuclear spins. As shown in Fig. 2 (orange data), we observed a single photoassociation line at a frequency of $\nu_0 =$ 281,445.045(60) GHz, where the error is the nominal uncertainty of the wavemeter. The linewidth of the photoassociation dip is 15 MHz, close to the natural linewidth of about 10 MHz. The next photoassociation line is expected 570 GHz away (*29*).

We then turned on the ion trap and repeated the experiment with an exposure time of 0.5 s (blue data). In addition to the strong photoassociation dip at $\nu = \nu_0$, a number of other loss dips were observed. As our analysis will show, these resonances belong to product molecules from three-body recombination that are state-selectively ionized as the probe laser is scanned. The ionized molecules were immediately trapped in the Paul trap, which was arranged to immerse them in the cold atom cloud. The ions undergo collisions with the atoms and induce atomic losses that can be substantial during exposure time. A larger number of ions leads

[1]Institut für Quantenmaterie and Center for Integrated Quantum Science and Technology IQST, Universität Ulm, 89069 Ulm, Germany. [2]Institut für Quantenoptik, Leibniz Universität Hannover, 30167 Hannover, Germany. [3]Joint Quantum Institute, University of Maryland, and the National Institute of Standards and Technology (NIST), College Park, MD 20742, USA. [4]American Physical Society, Ridge, NY 11961, USA. [5]JILA, NIST, and the Department of Physics, University of Colorado, Boulder, CO 80309, USA.
*Corresponding author. Email: johannes.denschlag@uni-ulm.de

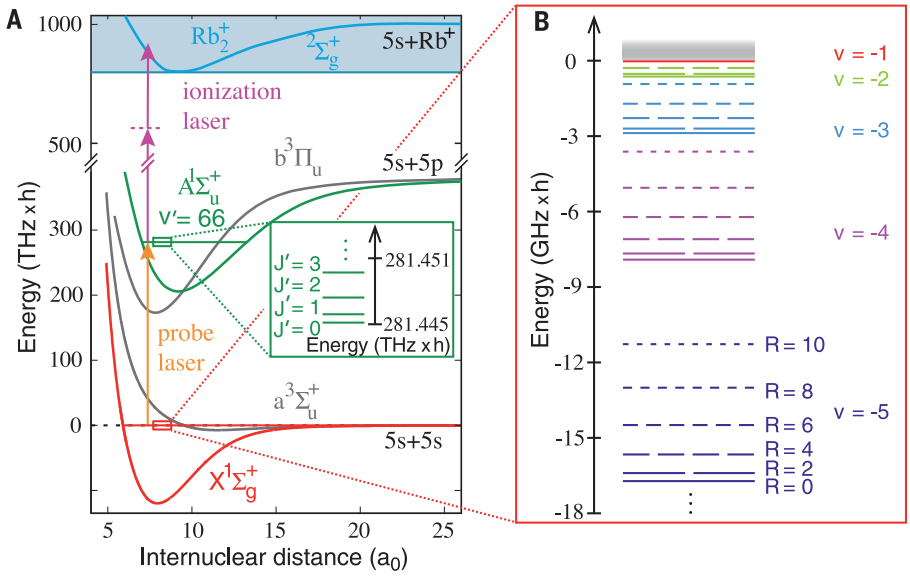

Fig. 1. REMPI scheme and overview of relevant molecular states. (**A**) A two-color (1, 2) REMPI scheme detects weakly bound molecules close to the 5s + 5s dissociation threshold. The probe laser drives a resonant transition toward the $A^1\Sigma_u^+$, $v' = 66$ vibrational level, which exhibits a simple rotational substructure (see inset). J' is the total angular momentum quantum number excluding nuclear spins. Afterward, two photons from the ionization laser ionize the molecule. a_0 is the Bohr radius. (**B**) Calculated energy levels of selected, weakly bound molecular states with the quantum numbers v and R for vibration and mechanical rotation, respectively. Only levels with total positive parity and angular momentum $F = 2$ that correlate to the $f_a = f_b = 1$ atomic asymptote are shown. This asymptote marks the zero energy reference level. The vibrational quantum number v is counted downwards starting at $v = -1$ for the most weakly bound vibrational state.

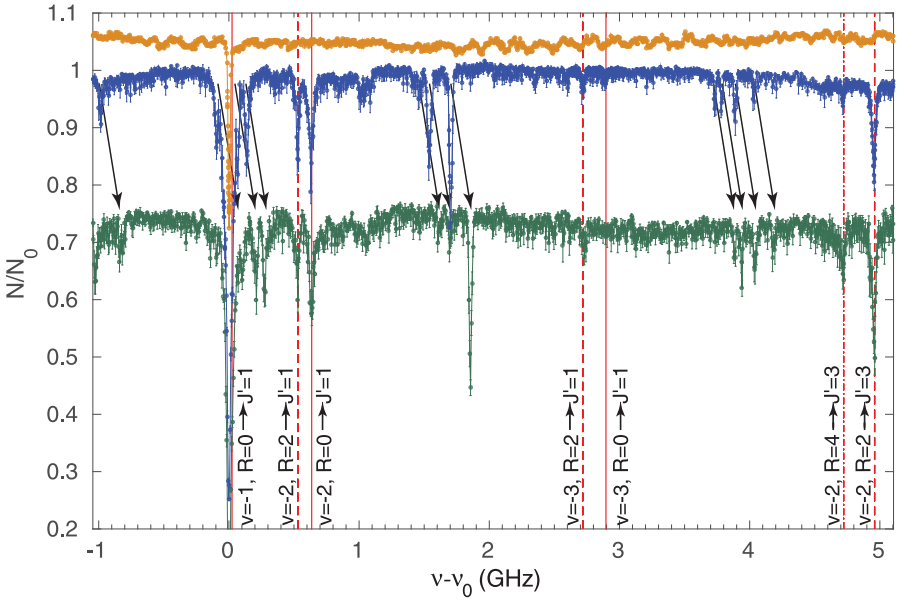

Fig. 2. Photoassociation and REMPI spectra. Shown is the remaining atom fraction N/N_0 as a function of the probe laser frequency ν, where N_0 is the number of remaining atoms for a far off-resonant probe laser. Orange data correspond to the photoassociation spectrum, with a single line at $\nu = \nu_0 \equiv 281{,}445.045$ GHz. For better visibility the record is shifted up by 0.05 units. The blue and green data are REMPI spectra. For the blue data, the ionization laser frequency is 281,629.15 GHz, whereas for the green data, the laser was red-shifted by 150 MHz. Each REMPI data point is the average of 10 repetitions, with the error bars representing the statistical standard deviation. For better visibility, the green spectrum is vertically shifted by −0.25 units, which cuts off part of its photoassociation line. The vertical lines mark assigned resonant transitions of the first REMPI step (v and R are vibrational and rotational quantum numbers). For black arrows, see text.

to a larger loss of atoms. Resonance dips in Fig. 2 with a depth of about 0.3 units are typically induced by an average of about five ions. This measurement of atomic loss constitutes a semiquantitative ion detection method which we refer to as ion detection scheme I (see supplementary materials for details).

We first consider REMPI transitions toward $A^1\Sigma_u^+$, $v' = 66$, $J' = 1$ and turn to $J' > 1$ afterwards. As the probe laser frequency increases, starting from ν_0, it probes increasingly deeply bound molecular levels. In the given frequency range of Fig. 2, we observed signals from the most weakly bound vibrational states $v = -1$, -2, and -3. The five vertical lines at $\nu - \nu_0 < 3$ GHz show the predicted resonance positions for the transitions indicated next to the lines, probing weakly bound states characterized by $f_a = f_b = 1$, $F = 2$, $R = 0$ and 2 (see also Fig. 1B). These predicted lines match our measured resonances within a few megahertz. We note that in the given spectrum, the signal corresponding to $v = -1$ is buried under the strong photoassociation line. As shown in fig. S2, however, it was clearly resolved in a refined scan. Some of the observed molecular states have nonvanishing rotational angular momentum R (see, e.g., $R = 4$ in Fig. 2). This is noteworthy, as at ultracold temperatures the atoms originally collide in s-waves where $R = 0$. The rotational excitation is due to an anisotropic interaction between the formed molecule and the remaining atom in the three-body collision complex.

As a consistency check of our assignment, we can make use of the fact that for molecules with $R > 0$, each level can give rise to two transition lines, $R \rightarrow J' = R \pm 1$. Indeed, we verified that, e.g., the level $v = -2$, $R = 2$ not only produces a transition line at ≈0.5 GHz ($J' = 1$) but also one at ≈5 GHz ($J' = 3$) (see Fig. 2). Both transition lines are of similar strength, as expected.

After determining that the observed resonance lines belong to weakly bound molecules in well-defined quantum states, one might still question whether the origin of the molecules is three-body recombination. We have performed test measurements on the density dependence of the ion signal for transition lines (see fig. S1). The ion signals normalized to the total atom numbers show a clear quadratic scaling behavior, which points to the three-body nature of the molecule formation.

Besides the weakly bound molecular states with the quantum numbers $f_a = f_b = 1$, there exist other states near threshold with the quantum numbers $f_a = f_b = 2$ or $f_{a/b} = 1, f_{b/a} = 2$ (see data S1 and S2). However, we only observed clear signals from $f_a = f_b = 1$ molecules in our measurements. Furthermore, we only observed molecules with an even rotational quantum number, i.e., $R = 0, 2, 4, \ldots$, which corresponds to positive total parity. The spin quantum numbers f_a and f_b, as well as the total parity of the product molecules, are the same as for the two-body atomic scattering state initially prepared in our experiment. The total parity of the scattering state must be even because the colliding atoms are identical bosons, and hence, their partial wave must be even. Thus, our present experiments indicate that the internal spin states of the colliding atoms do not change when a weakly bound molecule is formed in three-body recombination. This

is in contrast to our previous measurements where we investigated more deeply bound Rb_2 molecules and observed a broad range of spin states, including even and odd R (27). This apparent change in the propensity rule with increasing binding energy might be linked to the accidental near degeneracy of the weakly bound singlet and triplet levels of Rb_2, as explained in (26).

In addition to the assigned transition lines, several other unidentified resonance dips are visible in Fig. 2 (blue data). To investigate their origin, we measured the spectrum again, but with the ionization laser frequency shifted by –150 MHz (green data in Fig. 2). Both scans exhibit the already assigned transition lines at the same probe laser frequencies. The positions of several unidentified resonance dips, however, shifted by +150 MHz. Thus, for these dips, the sum of the ionization and probe laser frequencies remains constant. This indicates a two-photon process, where the combination of a probe and an ionization photon resonantly populates an intermediate molecular level. A third photon finally ionizes the molecule. Therefore, these transition lines correspond to a (2, 1) REMPI process. Currently, we have not yet assigned these lines to specific molecular transitions. We note that further unidentified resonance dips can be found in the spectrum, which, however, belong to more deeply bound states with other REMPI paths and need to be further analyzed.

Our spectroscopic method reveals fine details of hyperfine and exchange interaction in the molecular-level structure. Figure 3 shows the transitions $v = -3$, $R = 0, 2 \rightarrow J' = 1$, observed with ion detection scheme II (26), where the ions are first accumulated in a displaced ion trap and counted afterwards by means of the loss they inflict on a newly prepared atom cloud. Each of the $R = 0, 2$ levels consists of two ($F = 0$ and $F = 2$) hyperfine sublevels with a small splitting of about 20 MHz. [An additional substructure of these levels due to coupling of F to R is negligible (26).] The small splitting is linked to the fact that the singlet $X^1\Sigma_g^+$ and triplet $a^3\Sigma_u^+$ potentials have slightly different scattering lengths. The calculated transition frequencies are indicated as vertical lines in Fig. 3. In the spectrum, we only observe hyperfine levels with $F = 2$. From the peak heights and the noise,

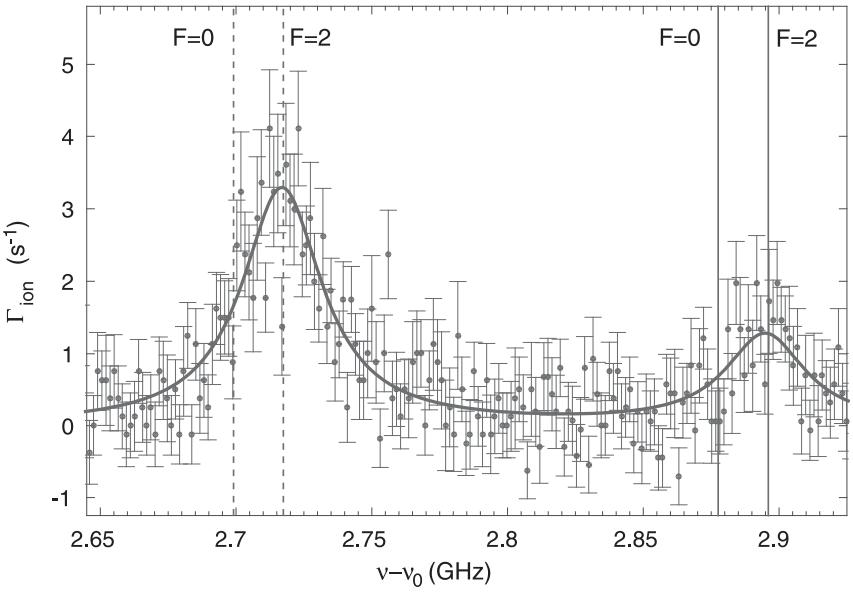

Fig. 3. Discrimination of hyperfine levels. The REMPI spectrum shows two transition lines to $J' = 1$, starting from the vibrational and rotational quantum numbers $v = -3$, $R = 0$ (peak on the right) and $v = -3$, $R = 2$ (peak on the left), respectively (see also, Fig. 2). Γ_{ion} is the ion production rate. The vertical lines show calculated positions of possible product signals with hyperfine quantum numbers $F = 0$ and 2. The data reveal that only $F = 2$ states are substantially populated. Each data point is the average of 43 repetitions, and error bars indicate the statistical standard deviation. The red solid line is a Lorentzian fit of the two transition lines. The fit was not weighted to the error bars and has a reduced chi-square value of $\chi^2 = 0.96$. As before, $\nu = 281{,}445.045$ GHz.

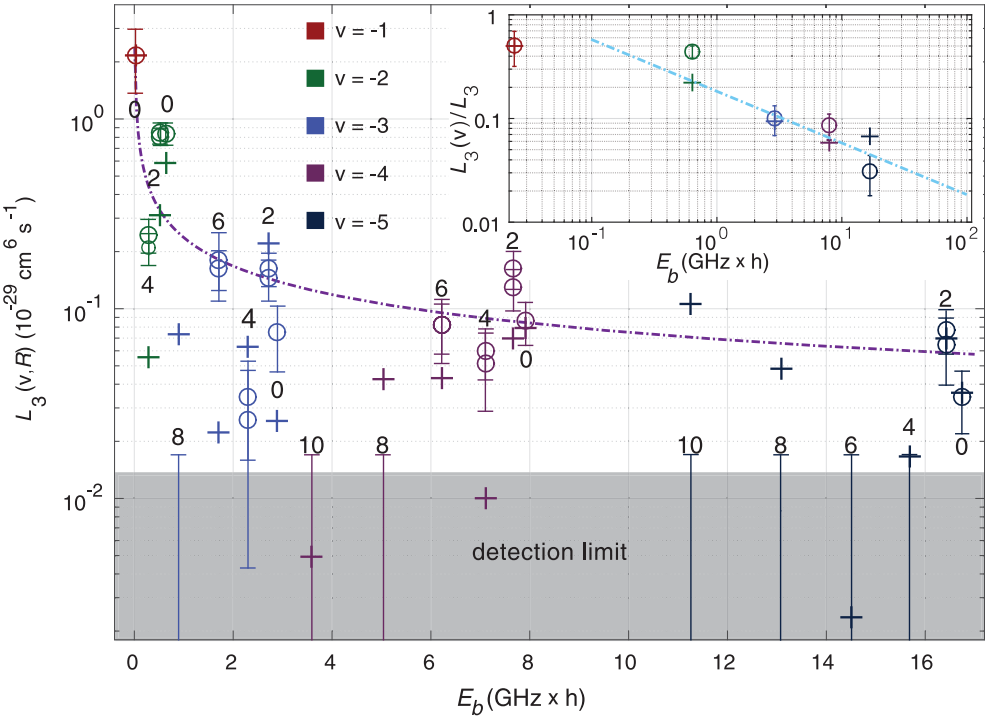

Fig. 4. Population distribution of molecular product states following three-body recombination. The plot shows the loss rate constants L_3 (v, R) due to three-body recombination into various molecular product channels, as specified by the quantum numbers v (vibration) and R (rotation) and the respective binding energy E_b. R is indicated next to the data points. All product channels belong to the $f_a = 1$, $f_b = 1$ atomic asymptote and have $F = 2$. Circles are measurements. Crosses are calculations, rescaled as described in (26). Error bars in the gray region indicate upper limits derived from the experimental noise level. Two circles for the same product channel correspond to REMPI transitions to two different excited levels, $J' = R \pm 1$. The inset presents the branching ratio into the five vibrational levels, calculated by summing over all respective rotational contributions and by normalizing with the total loss rate constant L_3. The dashed dotted lines (figure and inset) are proportional to $1/\sqrt{E_b}$. The error bars correspond to the statistical standard deviation.

we estimate that residual $F = 0$ signals must be smaller by at least a factor of four as compared to $F = 2$. In all other measurements for weakly bound molecules, we also found signatures only for levels with total internal spin $F = 2$. Interestingly, F is the same as that for the two-body scattering state. Thus, this finding supports our hypothesis that the molecular product has the same internal spin state as the two-body atomic scattering state.

We calibrated the ion signals to determine the three-body recombination–induced loss rate constants $L_3\ (v, R)$ for the flux into individual rovibrational levels in absolute terms. For this, we determined the probability that a molecule is ionized by the REMPI scheme once it has been formed (*26*). Figure 4 (circles) shows the individual loss rate constants $L_3\ (v, R)$ as inferred from our experimental data (*26*). This corresponds to the population distribution of molecular products. We investigated weakly bound molecular levels up to a binding energy of 17 GHz × h, where h is Planck's constant, as marked by vibrational and rotational quantum numbers in the plot. The observed lines can unambiguously be assigned to molecular product states as measurements, and calculated resonance frequencies accurately match within the experimental resolution of a few megahertz. Generally, the error bars shown in Fig. 4 represent the statistical uncertainties of the ion signals. We note, however, that additional large uncertainties arise, dominated by a global normalization error of up to 60% due to imperfect atom number calibration (*26*).

Our data show an overall tendency for the loss rate constants $L_3\ (v, R)$ to drop for increasing binding energies as anticipated for a dilute ultracold gas, but with fluctuations with R as discussed below. The decrease is not abrupt and roughly agrees with a $1/\sqrt{E_b}$ dependence, where E_b is the binding energy. The $1/\sqrt{E_b}$ dependence is a simple propensity rule that can be tested further in future research. To better understand the measured population distribution, we have also carried out state-of-the-art numerical three-body calculations (crosses in Fig. 4) based on a simplified model of long-range potentials (*26*). In agreement with the data, we find again the $1/\sqrt{E_b}$ dependence for $L_3\ (v, R)$.

For a fixed v, both theory and experiment show large variations of $L_3\ (v, R)$ with R. In particular, the $R = 4$ signals are generally suppressed with respect to the $R = 2$ signals for a given vibrational level. This is also supported by our calculations, which suggest that the variation of population with R is oscillatory. In general, variations as a function of R are expected because the state-to-state S-matrix elements will be influenced by multiple paths and Stückelberg oscillations associated with one or more curve crossings in the adiabatic potential curves, as indicated in (*3*, *16*, *17*) (see also fig. S6). In the experiment we observe rotational angular momenta up to $R = 6$. Theory predicts a population of even higher rotational quantum numbers. In our calculations, the variations for the $v = -2$ and -3 levels seem to have converged with respect to increasing the number of $R = 0$ bound states in the model [see (*26*)]. However, the $v = -4$ and -5 rotational distributions have not yet fully converged with respect to adding bound states. Thus, the rotational distribution for these more deeply bound levels is sensitive to shorter-range details that our model is not treating fully. Despite these limitations, the theoretical model suggests that the rotational distributions for given v might have nonnegligible sensitivity to three-body corrections that are not pairwise additive (*26*). In general, the sum $L_3\ (v) = \sum_R L_3\ (v, R)$ over all rotational contributions for a given v might be less subject to variation. The inset in Fig. 4 presents the measured and calculated values of $L_3\ (v)$ for the individual vibrational levels, normalized to the total loss rate of $L_3 = (4.3 \pm 1.8) \times 10^{-29}\ \mathrm{cm}^6\ \mathrm{s}^{-1}$ determined by Burt *et al.* (*12*). Indeed, the results show a similar qualitative drop off tracking near a line that varies as $1/\sqrt{E_b}$. According to the given normalization, the measurements reveal that roughly 50% of all molecules produced through three-body recombination are formed in level $v = -1$. We can estimate that about 10% of the molecules are more deeply bound than at $v = -5$, using the $1/\sqrt{E_b}$ scaling law for the vibrational population. The total population of levels $v < -5$ is then approximately given by $\sum_{i<-5} E_b\ (v)^{-1/2} \Big/ \sum_v E_b\ (v)^{-1/2}$. Here, $E_b\ (v)$ is the calculated $R = 0$ bound-state energy for the vibrational level v of the mixed $a^3\Sigma_u^+$ state. Indeed, some of the more deeply bound levels were observed in (*27*).

Our experimental scheme can readily be adapted to other bosonic or fermionic elements or isotopes. In general, the product measurement technique introduced here can be used to investigate a wide range of inelastic processes at ultralow temperatures well beyond three-body recombination, such as molecular relaxation and rearrangement reactions. Therefore, the present work sets the stage for experiments in which chemical reactions and inelastic collisions can be explored in a state-to-state fashion, with full resolution on the quantum level.

REFERENCES AND NOTES

1. Y. Wang, J. P. D'Incao, B. D. Esry, *Phys. Rev. A* **83**, 032703 (2011).
2. J. F. E. Croft *et al.*, *Nat. Commun.* **8**, 15897 (2017).
3. J. Wang, J. P. D'Incao, C. H. Greene, *Phys. Rev. A* **84**, 052721 (2011).
4. X. Yang, *Annu. Rev. Phys. Chem.* **58**, 433–459 (2007).
5. J. Jankunas, A. Osterwalder, *Annu. Rev. Phys. Chem.* **66**, 241–262 (2015).
6. S. Y. T. van de Meerakker, H. L. Bethlem, N. Vanhaecke, G. Meijer, *Chem. Rev.* **112**, 4828–4878 (2012).
7. A. J. Moerdijk, H. M. J. M. Boesten, B. J. Verhaar, *Phys. Rev. A* **53**, 916–920 (1996).
8. P. O. Fedichev, M. W. Reynolds, G. V. Shlyapnikov, *Phys. Rev. Lett.* **77**, 2921–2924 (1996).
9. J. Söding *et al.*, *Appl. Phys. B* **69**, 257–261 (1999).
10. G. Quéméner, P. S. Julienne, *Chem. Rev.* **112**, 4949–5011 (2012).
11. C. Chin, R. Grimm, P. Julienne, E. Tiesinga, *Rev. Mod. Phys.* **82**, 1225–1286 (2010).
12. E. A. Burt *et al.*, *Phys. Rev. Lett.* **79**, 337–340 (1997).
13. A. Krükow *et al.*, *Phys. Rev. Lett.* **116**, 193201 (2016).
14. Z. Shotan, O. Machtey, S. Kokkelmans, L. Khaykovich, *Phys. Rev. Lett.* **113**, 053202 (2014).
15. T. Kraemer *et al.*, *Nature* **440**, 315–318 (2006).
16. B. D. Esry, C. H. Greene, J. P. Burke, *Phys. Rev. Lett.* **83**, 1751–1754 (1999).
17. J. P. D'Incao, B. D. Esry, *Phys. Rev. Lett.* **94**, 213201 (2005).
18. D. S. Petrov, *Phys. Rev. Lett.* **93**, 143201 (2004).
19. J. Pérez-Ríos, S. Ragole, J. Wang, C. H. Greene, *J. Chem. Phys.* **140**, 044307 (2014).
20. Y. Wang, P. S. Julienne, *Nat. Phys.* **10**, 768–773 (2014).
21. E. Braaten, H.-W. Hammer, *Phys. Rep.* **428**, 259–390 (2006).
22. T. Weber, J. Herbig, M. Mark, H.-C. Nägerl, R. Grimm, *Phys. Rev. Lett.* **91**, 123201 (2003).
23. S. Jochim *et al.*, *Phys. Rev. Lett.* **91**, 240402 (2003).
24. D. J. Nesbitt, *Chem. Rev.* **112**, 5062–5072 (2012).
25. M. L. González-Martínez, O. Dulieu, P. Larrégaray, L. Bonnet, *Phys. Rev. A* **90**, 052716 (2014).
26. Materials and methods are available as supplementary materials.
27. A. Härter *et al.*, *Nat. Phys.* **9**, 512–517 (2013).
28. A. Drozdova *et al.*, *Phys. Rev. A* **88**, 022504 (2013).
29. M. Deiß, B. Drews, J. Hecker Denschlag, E. Tiemann, *New J. Phys.* **17**, 083032 (2015).
30. K. M. Jones, E. Tiesinga, P. D. Lett, P. S. Julienne, *Rev. Mod. Phys.* **78**, 483–535 (2006).

ACKNOWLEDGMENTS

This work was supported by the German Research Foundation (DFG, Deutsche Forschungsgemeinschaft) within SFB/TRR21 and grant DE 510/2-1. A.K. acknowledges support from the Carl Zeiss foundation. E.T. acknowledges support from the Minister of Science and Culture of Lower Saxony, Germany, by providing a Niedersachsenprofessur (Lower Saxony professorship). J.P.D. acknowledges NSF funding (grant PHY-1607204). J.H.D., P.S.J., E.T., B.P.R., Y.W., and J.P.D. acknowledge support from several Kavli Institute for Theoretical Physics programs (NSF grant PHY-1125915). J.H.D. would like to thank D. Nesbit for insightful encouragement. The measured data presented in this paper are available from the corresponding author upon reasonable request. Data S1 and S2 provide tables for term energies and quantum numbers of Rb_2 levels in the mixed electronic states $X^1\Sigma_g^+$ and $a^3\Sigma_u^+$ with negative and positive total parity, respectively. Data S3 to S5 contain the data plotted in Figs. 2 to 4. J.W., A.K., and M.D. carried out the experiments. E.T. carried out coupled-channel calculations for Rb_2. B.P.R., J.P.D., Y.W., and P.S.J. set up, implemented, and analyzed the three-body calculations. J.H.D. supervised the project. All authors contributed to the analysis of the experiment and to the writing of the manuscript. The authors declare no competing financial interests.

SUPPLEMENTARY MATERIALS

www.sciencemag.org/content/358/6365/921/suppl/DC1
Materials and Methods
Figs. S1 to S7
References (*31*–*41*)
Data S1 to S5

31 May 2017; accepted 10 October 2017
10.1126/science.aan8721

State-to-state chemistry for three-body recombination in an ultracold rubidium gas

Joschka Wolf, Markus Deiß, Artjom Krükow, Eberhard Tiemann, Brandon P. Ruzic, Yujun Wang, José P. D'Incao, Paul S. Julienne and Johannes Hecker Denschlag

Science **358** (6365), 921-924.
DOI: 10.1126/science.aan8721

Tracking a trio of rubidium atoms

Crossed molecular beams have provided decades' worth of knowledge into how quantum mechanics governs chemical reactivity. Nonetheless, the technique is generally limited to the collision of two partners. Wolf *et al.* report on a three-body process with full quantum state resolution. By cooling rubidium atoms to ultralow temperatures in an optical trap, they were able to observe dimer formation, stabilized by collision with a third atom, and extract the precise dependence of product states on the initial states of the atoms involved.

Science, this issue p. 921